Geosci. Model Dev. Discuss., https://doi.org/10.5194/gmd-2018-281
Manuscript under review for journal Geosci. Model Dev.
Discussion started: 4 February 2019

Geoscientific Model Development Discussions
Open Access
EGU

University of Warsaw Lagrangian Cloud Model (UWLCM) 1.0: a modern Large-Eddy Simulation tool for warm cloud modeling with Lagrangian microphysics

Piotr Dziekan, Maciej Waruszewski, and Hanna Pawlowska
Institute of Geophysics, Faculty of Physics, University of Warsaw, Poland
Correspondence: Piotr Dziekan (pdziekan@fuw.edu.pl)

Abstract. A new anelastic large-eddy simulation model with an Eulerian dynamical core and a Lagrangian particle-based microphysics is presented. The dynamical core uses the MPDATA advection scheme and the generalized conjugate residual pressure solver, while the microphysics scheme is based on the Super-Droplet Method. Algorithms for coupling of the Lagrangian microphysics with the Eulerian dynamics are presented, including spatial and temporal discretizations and a condensation sub-stepping algorithm. The model is free of numerical diffusion in the droplet size spectrum. Activation of droplets is modeled explicitly, making the model less sensitive to local supersaturation maxima than models in which activation is parametrised. Simulations of a drizzling marine stratocumulus give results in agreement with other LES models. Relatively low number of computational particles is sufficient to obtain the correct averaged properties of a cloud. High computational performance is achieved thanks to the use of GPU accelerators.

1 Introduction

In the last decade, Lagrangian particle-based cloud microphysics schemes have been drawing increasing attention. They are similar to the Eulerian bin schemes in that they explicitly model the size spectrum of droplets and explicitly resolve microphysical processes, but have a number of advantages over them (Grabowski et al., 2018b). One of the advantages is that the Lagrangian schemes have no numerical diffusion in the spectrum of droplet sizes. Several Lagrangian schemes for warm cloud microphysics have been developed so far (Andrejczuk et al., 2008; Shima et al., 2009; Riechelmann et al., 2012). Arguably, the most important difference between these schemes is in the way collision-coalescence is modeled. The coalescence algorithm used in the Super-Droplet Method (SDM) of Shima et al. (2009) seems to be most promising, as it was found to be the most accurate of the coalescence algorithms used in various Lagrangian microphysics schemes (Unterstrasser et al., 2017, where it is called the "all-or-nothing" algorithm). A numerical implementation of the SDM is a major part of the libcloudph++ library (Arabas et al., 2015) developed by the cloud modeling group at the University of Warsaw.

In this paper, we document development of a new Large-Eddy Simulation (LES) model called the University of Warsaw Lagrangian Cloud Model (UWLCM). It is an anelastic model with a finite-difference Eulerian dynamical core and a Lagrangian microphysics. The Lipps-Hemler anelastic approximation (Lipps and Hemler, 1982) is used, which is applicable to a wide range of atmospheric flows (Klein et al., 2010; Smolarkiewicz, 2011). The dynamical core is built on top of the libmpdata++

Geosci. Model Dev. Discuss., https://doi.org/10.5194/gmd-2018-281
Manuscript under review for journal Geosci. Model Dev.
Discussion started: 4 February 2019

Geoscientific Model Development Discussions
Open Access
EGU

library (Jaruga et al., 2015) also developed by the cloud modeling group at the University of Warsaw. libmpdata++ is a collection of solvers for the generalized transport equation. In libmpdata++, advection is modeled using the multidimensional positive-definite advection transport algorithm (MPDATA) – see Smolarkiewicz (2006) for a recent review. Liquid water is modeled with the Lagrangian SDM implemented in libcloudph++. We do not assume any artificial categorization of liquid water particles. In consequence, all particles, i.e. humidified aerosols, cloud droplets and rain drops, evolve according to the same set of basic equations.

One of the key reasons for developing a new model is to use a modern software development approach. All of the code is written in the C++ language and makes use of many mature libraries available in that language (e.g. Blitz++, Boost, Thrust). The code is open-source and under a version-control system. A set of automated tests greatly simplifies code development. UWLCM makes efficient use of modern computers, that have both central processing units (CPUs) and graphics processing units (GPUs). The Eulerian computations of the dynamical core are done on CPUs and, simultaneously, the Lagrangian microphysical computations are done on GPUs. However, it is also possible to run the Lagrangian microphysics on CPUs.

Some results obtained using earlier versions of UWLCM are already published. In Grabowski et al. (2018a), UWLCM was used to model a 2-dimensional moist thermal and in Grabowski et al. (2018b), an idealized 3-dimensional cumulus cloud was modeled. Here, we present simulations of a drizzling marine stratocumulus using the DYCOMS-II RF02 setup. UWLCM results are compared with 11 LES models that took part in the Ackerman et al. (2009) intercomparison. It is of particular interest how much drizzle a LES model with Lagrangian microphysics produces, compared to models with bin or bulk microphysics that took part in the intercomparison. To our knowledge, LES simulations with warm cloud Lagrangian microphysics were used to study drizzling stratocumulus only by Andrejczuk et al. (2008, 2010). This type of models was more often employed to study cumulus clouds (Riechelmann et al., 2012; Naumann and Seifert, 2015; Arabas and Shima, 2013; Hoffmann et al., 2015, 2017).

Section 2 presents the governing equations of the model, section 3 describes the numerical algorithms for solving these equations, the stratocumulus simulation results are discussed in section 4, and section 5 contains a summary and planned developments of the model. A list of symbols used and their definitions are given in appendix A, appendix B defines the two sub-stepping algorithms tested in the paper and appendix C contains a brief description of the software implementation of the model.

2 Governing equations

2.1 Eulerian variables

Eulerian prognostic variables of the model are the potential temperature θ, water vapor mixing ratio q_v and air velocity $\boldsymbol{u}$. Equations governing time evolution of these variables are obtained through the Lipps-Hemler approximation, which relies on the assumption that atmosphere does not depart far from some stationary state, called the *reference* state (Lipps and Hemler, 1982). The reference state is assumed here to be a dry, hydrostatically balanced state with constant stability S^r. S^r is equal to the average stability of the sounding used to initialize the simulation. Surface density and pressure of the reference state

Geosci. Model Dev. Discuss., https://doi.org/10.5194/gmd-2018-281
Manuscript under review for journal Geosci. Model Dev.
Discussion started: 4 February 2019

Geoscientific Model Development Discussions

are equal to those of the initial sounding. Vertical profiles of potential temperature and density of dry air in the reference state are (Clark and Farley, 1984):

$$\theta^r(z) = \theta_v^0 \exp(S^r z), \tag{1}$$

$$\rho_d^r(z) = \rho^0 \exp(-S^r z) \left[1 - \frac{g}{c_{pd} S^r \theta_v^0} (1 - \exp(-S^r z))\right]^{(c_{pd}/R_d)-1}, \tag{2}$$

where θ_v^0 and ρ^0 are values of the virtual potential temperature and of the air density taken from the initial sounding at the ground level. An auxiliary *environmental* state is introduced to increase precision of numerical calculations (Smolarkiewicz et al., 2014). It is a hydrostatically balanced moist state with stationary profiles $\theta^e(z)$, $p^e(z)$, $T^e(z)$, $q_v^e(z)$ and $q_l^e(z)$ calculated from the initial sounding. If the initial sounding is supersaturated, all supersaturation is assumed to be condensed in the environmental state.

The set of anelastic Lipps-Hemler equations (Lipps and Hemler, 1982; Grabowski and Smolarkiewicz, 1996; Clark and Farley, 1984) that govern time evolution of the Eulerian prognostic variables is

$$D_t \boldsymbol{u} = -\nabla \pi + \boldsymbol{k} B + \boldsymbol{F}_u, \tag{3}$$

$$D_t \theta = \frac{\theta^e}{T^e} \left(\frac{l_v}{c_{pd}} C \right) + F_\theta, \tag{4}$$

$$D_t q_v = -C + F_{q_v}, \tag{5}$$

where D_t denotes the material derivative: $D_t = \partial_t + \boldsymbol{u} \cdot \nabla$. Following Grabowski and Smolarkiewicz (1996), the buoyancy is defined as

$$B = g \left[\frac{\theta - \theta^e}{\theta^r} + \epsilon (q_v - q_v^e) - (q_l - q_l^e) \right]. \tag{6}$$

The condensation rate C in eqs. (4) and (5) and the liquid water mixing ratio q_l in eq. (6) come from the Lagrangian microphysics scheme. The terms F_* represent a total forcing due to surface fluxes, radiative heating/cooling, large-scale subsidence and absorbers. The dry-air density is assumed to be equal to the reference state density profile ρ_d^r and, what is characteristic for the anelastic approximation, dry-air density at given position does not change with time: $\partial_t \rho_d^r = 0$. By putting $\partial_t \rho_d^r = 0$ into the continuity equation, the following constraint on the velocity field is obtained:

$$\nabla \cdot (\rho_d^r \boldsymbol{u}) = 0, \tag{7}$$

which will be referred to as the *anelastic constraint*. Throughout the model, the pressure is assumed to be equal to the environmental pressure profile $p^e(z)$. The only exception is the pressure gradient term appearing in eq. (3), in which the pressure is adjusted so that $\boldsymbol{u}$ satisfies the anelastic constraint (eq. 7) (Lipps and Hemler, 1982; Grabowski and Smolarkiewicz, 1996).

2.2 Lagrangian particles

Liquid water is modeled with a Lagrangian, particle-based microphysics scheme of libcloudph++ (Arabas et al., 2015). It is an implementation of the Super-Droplet Method (SDM) (Shima et al., 2009). The key idea is to represent all liquid particles using

Geosci. Model Dev. Discuss., https://doi.org/10.5194/gmd-2018-281
Manuscript under review for journal Geosci. Model Dev.
Discussion started: 4 February 2019

Geoscientific Model Development Discussions

a small number of computational particles, called super-droplets (SDs). Each SD represents a large number of real particles. The number of real particles represented by a given SD is called the multiplicity (also known as the weighting factor), and is denoted by ξ. Other attributes of SDs are the dry radius r_d, wet radius r, hygroscopicity parameter κ and position $\boldsymbol{x}$ in the model domain.

The condensational growth rate of a SD is equal to that of a single real particle. We calculate it using the Maxwell-Mason approximation (see Arabas et al. 2015):

$$r\frac{dr}{dt} = \frac{D'_{\text{eff}}}{\rho_w}\left(1 - \frac{a_w\left(r, r_d, \kappa\right)\exp(A/r)}{\phi}\right), \tag{8}$$

where

$$\frac{1}{D'_{\text{eff}}} = \left(D\rho_d q_v\right)^{-1} + K^{-1}\frac{1}{\phi}\frac{l_v}{T}\left(\frac{l_v}{R_v T} - 1\right), \tag{9}$$

water activity is calculated using the κ-Köhler parametrisation (Petters and Kreidenweis, 2007):

$$a_w\left(r, r_d, \kappa\right) = \frac{r^3 - r_d^3}{r^3 - r_d^3\left(1-\kappa\right)} \tag{10}$$

and, following Lipps and Hemler (1982), the relative humidity is defined as $\phi = q_v/q_{vs}$, with the saturation water vapor mixing ratio calculated using the formula $q_{vs} = 0.622 e_s/\left(p^e - e_s\right)$. Formulas for the parameters appearing in eqs. (8) and (9) can be found in Arabas et al. (2015). The vapor and heat diffusion coefficients D and K are evaluated as in Arabas and Pawlowska (2011) (see eqs. 20 and 21 therein).

Collision-coalescence of droplets is treated as a stochastic process (Gillespie, 1972). Collision are possible only between droplets that are located within the same spatial cell, called the coalescence cell. It is assumed that coalescence cells are well-mixed, i.e. that droplets are randomly and uniformly distributed within a coalescence cell. Then, the probability that any two droplets j and k, which are located in the same coalescence cell, collide during the time interval Δt_{c} is given by the equation (Shima et al., 2009)

$$P_{j,k} = K_{j,k}\frac{\Delta t_{\text{c}}}{\Delta V}, \tag{11}$$

where $K_{j,k}$ is the coalescence kernel for these two droplets and ΔV is the volume of the coalescence cell. Probability of a collision between SDs needs to be increased to account for the fact that each SD represents a large number of real droplets. Probability that any two SDs j and k, which are in the same coalescence cell, collide during the time interval Δt_{c} is related to the probability of collision of real droplets in the following manner (Shima et al., 2009):

$$P_{j,k}^{\text{SD}} = \max\left(\xi_j, \xi_k\right) P_{j,k}. \tag{12}$$

Coalescence of the two SDs is interpreted as a coalescence of ξ_j pairs of real droplets. Each pair consists of one real droplet represented by the j-th SD and one real droplets represented by the k-th SD and SDs are labeled so that $\xi_j \leq \xi_k$. The remaining $\xi_k - \xi_j$ real droplets represented by the k-th SD are not affected by coalescence of these two SDs. Such treatment of coalescence,

Geosci. Model Dev. Discuss., https://doi.org/10.5194/gmd-2018-281
Manuscript under review for journal Geosci. Model Dev.
Discussion started: 4 February 2019

Geoscientific Model Development Discussions

sometimes referred to as the *all-or-nothing* algorithm, assures that the number of SDs does not increase due to the collision-coalescence. This algorithm was found to give the best results in a recent comparison of various coalescence algorithms used in Lagrangian schemes for microphysics (Unterstrasser et al., 2017). Dziekan and Pawlowska (2017) showed that the *all-or-nothing* algorithm produces correct realizations of the stochastic coalescence process described in (Gillespie, 1972), but only for $\xi = 1$. For $\xi > 1$, an average over realizations of the *all-or-nothing* algorithm is in good agreement with the expected value of the stochastic process, but the variability between realizations is much higher. This is because the number of SDs is much smaller than the number of real droplets. In consequence, the statistical sample for $\xi > 1$ is much smaller than in the more realistic case of $\xi = 1$. The collision-coalescence algorithm is not the only cause of the high variability for $\xi > 1$. The motion of SDs is also expected to give a high variability, because when a SD moves from one spatial cell to another, a large number of real particles is abruptly moved between these cells. It is not certain if the high variability in the SDM associated with collision-coalescence of SDs and motion of SDs has some impact on averaged properties of a modeled cloud. To determine if it does have an effect, we conduct simulations for various number of SDs (see section 4.2).

Super-droplets are treated as non-inertial particles that always sediment with the terminal velocity. The velocity of a SD is equal to $\boldsymbol{u}_{SD} = \boldsymbol{u} + (0, 0, w_t) + (0, 0, w_{\mathrm{LS}})$. This formula represents the combined effects of advection by air flow, sedimentation and large-scale subsidence.

3 Numerical algorithms

3.1 Numerical integration of Eulerian equations

Numerical integration of the governing Eulerian equations is done using the MPDATA algorithm implemented in libmpdata++ (Jaruga et al., 2015). MPDATA is an algorithm for solving the generalized transport equation (Smolarkiewicz, 2006)

$$\partial_t \left(G\psi\right) + \nabla \cdot \left(G\boldsymbol{u}\psi\right) = GR, \tag{13}$$

where ψ is a scalar field advected by the velocity field $\boldsymbol{u}$, R is the source/sink right-hand side (RHS) and G can represent the fluid density, the Jacobian of coordinate transformation or their product. The equivalent of eq. (13) in the Lagrangian description is:

$$\partial_t \psi + \boldsymbol{u} \cdot \nabla \psi = R. \tag{14}$$

Equation (3) for components of vector $\boldsymbol{u}$ and eqs. (4) and (5) have the same form as eq. (14). Equation (14) introduces notation that is convenient for presenting the numerical integration procedure of UWLCM. All RHS terms, except buoyancy and pressure gradient terms in eq. (3), are integrated with the forward Euler method. These terms are denoted by R_{E}. The buoyancy and pressure gradient terms, denoted by R_{T}, are applied using the trapezoidal rule. The integration algorithm is:

$$\psi^{[n+1]} = ADV\left(\psi^{[n]} + \Delta t R_{\mathrm{E}}^{[n]} + 0.5\Delta t R_{\mathrm{T}}^{[n]}, \boldsymbol{u}^{[n+1/2]}\right) + 0.5\Delta t R_{\mathrm{T}}^{[n+1]}, \tag{15}$$

Geosci. Model Dev. Discuss., https://doi.org/10.5194/gmd-2018-281
Manuscript under review for journal Geosci. Model Dev.
Discussion started: 4 February 2019

Geoscientific Model Development Discussions

where $ADV\left(\psi, \boldsymbol{u}\right)$ is an operator representing MPDATA advection of a scalar field ψ by the velocity field $\boldsymbol{u}$. Superscripts denote the time level. The mid-time-level velocity field $\boldsymbol{u}^{[n+1/2]}$ is obtained by linear extrapolation from $\boldsymbol{u}^{[n-1]}$ and $\boldsymbol{u}^{[n]}$.

It is characteristic for anelastic models that the pressure perturbation does not follow the ideal gas law, but is adjusted so that the velocity field satisfies eq. (7). By applying eq. (7) to the equation for $\boldsymbol{u}^{[n+1]}$ discretized in the form of eq. (15), the following elliptic equation for $\pi^{[n+1]}$ is obtained:

$$\nabla \cdot \left[\rho_d^r \left(\hat{\boldsymbol{u}} + 0.5\Delta t \boldsymbol{k} B^{[n+1]} - 0.5\Delta t \nabla \pi^{[n+1]}\right)\right] = 0, \tag{16}$$

where

$$\hat{\boldsymbol{u}} = ADV\left(\boldsymbol{u}^{[n]} + \Delta t \boldsymbol{F}_u^{[n]} + 0.5\Delta t \left(-\nabla \pi^{[n]} + \boldsymbol{k} B^{[n]}\right), \boldsymbol{u}^{[n+1/2]}\right), \tag{17}$$

and the thermodynamic fields required in $B^{[n+1]}$ are already available when the equation has to be solved. The pressure problem stated in eq. (16) is solved with the generalized conjugate residual solver (Smolarkiewicz and Margolin, 2000; Smolarkiewicz and Szmelter, 2011).

3.2 Numerical algorithms for super-droplets

For numerical reasons the condensational growth of SDs is solved in terms of the squared wet radius, as advocated by Shima et al. (2009). Integration of eq. (8) is done with a scheme that is implicit with respect to the wet radius and explicit with respect to q_v and θ:

$$r^{2[n+1]} = r^{2[n]} + \Delta t \left.\frac{dr^2}{dt}\right|_{r^{2[n+1]}, q_v^{[n]}, \theta^{[n]}}. \tag{18}$$

Solution for eq. (18) is found with a predictor-corrector procedure. We refer the reader to Arabas et al. (2015) for details of this procedure. Condensation is a fast process and the above procedure converges for time steps of around 0.1s. A typical time step Δt of a LES model is around 1s. Therefore it is necessary to do several condensation time steps in a single LES time step, what we call sub-stepping. To explain the idea of the sub-stepping algorithm, we introduce the following notation: S_c for the number of sub-steps, $\boldsymbol{\psi} = (\theta, q_v)$ for a vector of the Eulerian variables, $\boldsymbol{\psi}_{\text{old}}$ for values of the Eulerian variables after the sub-stepping algorithm finished in the previous time step and $\boldsymbol{\psi}_{\text{new}}$ for values of the Eulerian variables before the start of the sub-stepping algorithm in the current time step. In the first sub-step, the Eulerian variables are set to $\boldsymbol{\psi}_{\text{old}} + \frac{\boldsymbol{\psi}_{\text{new}} - \boldsymbol{\psi}_{\text{old}}}{S_c}$ and then condensation is calculated using the procedure defined in eq. (18). Please note that this condensation procedure changes the Eulerian variables. In each subsequent time step, $\frac{\boldsymbol{\psi}_{\text{new}} - \boldsymbol{\psi}_{\text{old}}}{S_c}$ is added to the Eulerian variables and then the condensation procedure is run again. Two types of the sub-stepping algorithm are considered, which differ only in the spatial cell from which the value of $\boldsymbol{\psi}_{\text{old}}$ is diagnosed. In the *per-particle* algorithm, $\boldsymbol{\psi}_{\text{old}}$ is diagnosed from the cell in which given SD was in the *previous* time step. In the *per-cell* algorithm, $\boldsymbol{\psi}_{\text{old}}$ is diagnosed from the cell in which given SD is in the *current* time step. The *per-cell* algorithm is less accurate, but computationally less demanding, because $\boldsymbol{\psi}_{\text{old}}$ is the same for all SDs that are in the same spatial cell. This is not true in the *per-particle* algorithm, in which $\boldsymbol{\psi}_{\text{old}}$ can be different for different SDs in the same cell, so each SD needs to remember its own value of $\boldsymbol{\psi}_{\text{old}}$. Moreover, in the *per-particle* algorithm, values of pressure and

Geosci. Model Dev. Discuss., https://doi.org/10.5194/gmd-2018-281
Manuscript under review for journal Geosci. Model Dev.
Discussion started: 4 February 2019

Geoscientific Model Development Discussions
Open Access
EGU

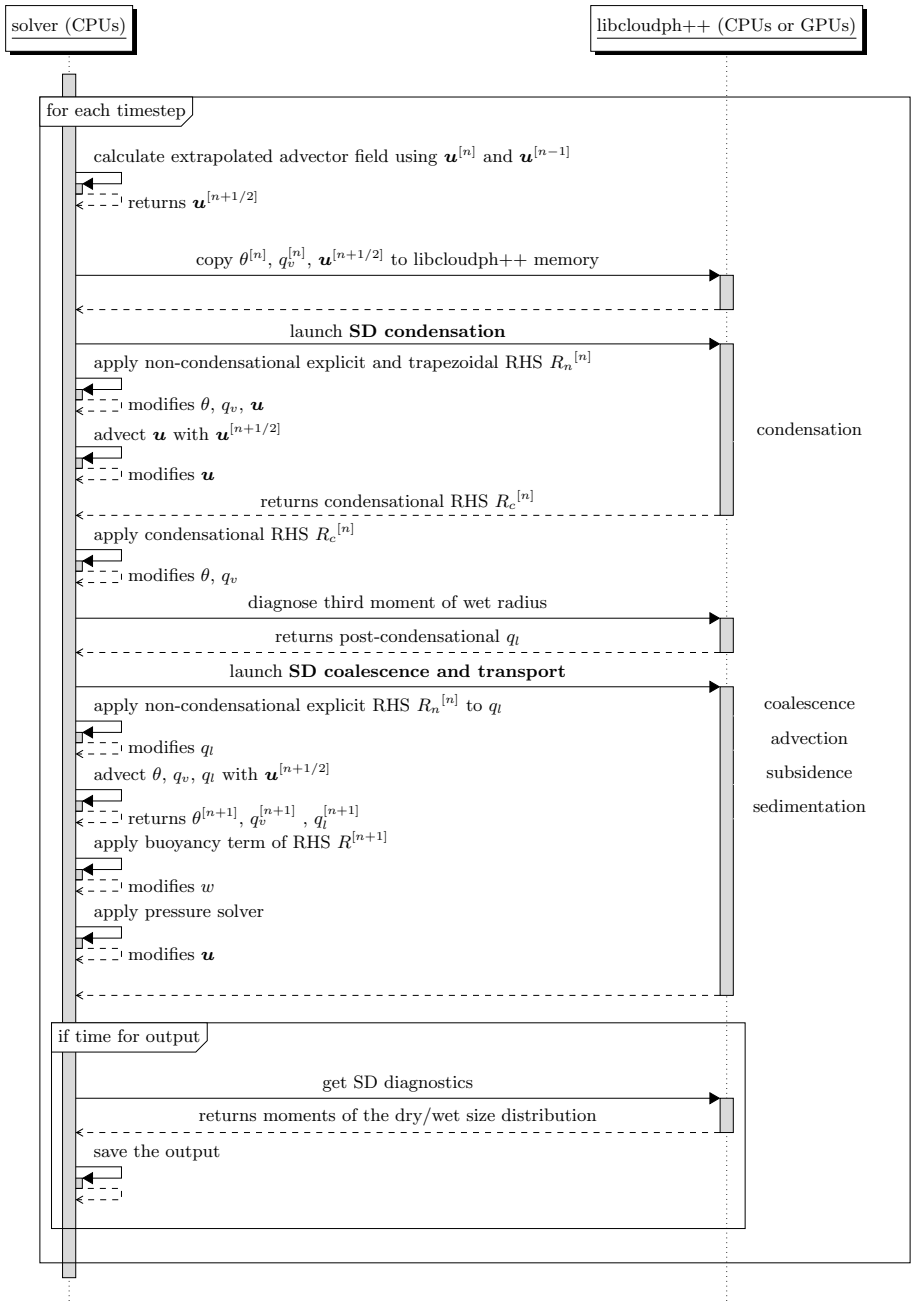

Figure 1. UML sequence diagram showing the order of operations within a single time step. Calls in boldface start microphysical calculations that are done on GPUs simultaneously with solver operations done on CPUs. The RHS is divided into condensational and non-condensational parts, $R = R_n + R_c$.

Geosci. Model Dev. Discuss., https://doi.org/10.5194/gmd-2018-281
Manuscript under review for journal Geosci. Model Dev.
Discussion started: 4 February 2019

density also need to vary between sub-steps. This is not necessary in the *per-cell* algorithm, because pressure and density are constant in time. Both sub-stepping algorithms are tested in section 4.2 to determine if the *per-cell* algorithm is sufficient, or is the *per-particle* sub-stepping necessary. A more detailed description of the sub-stepping algorithms is given in appendix B.

The stochastic collision-coalescence process described in section 2.2 is modeled with a Monte Carlo algorithm developed by Shima et al. (2009). The key feature of this algorithm is that each SD can collide only with one other SD during a time step. Thanks to that, the computational cost of the algorithm scales linearly, and not quadratically, with the number of SDs. Dziekan and Pawlowska (2017) showed that this "linear sampling" technique does not affect the mean, nor the standard deviation, of the results. Note that in the coalescence algorithm of Shima et al. (2009), a pair of SDs can collide multiple times during one time step. This feature was not implemented in libcloudph++ at the time when the paper Arabas et al. (2015) was published. libcloudph++ has been modified since then and now multiple collisions are allowed.

The procedure for initialization of SD sizes is described in detail in Dziekan and Pawlowska (2017), where it is called the "constant SD" initialization. In short, the range of initial values of r_d is divided into N_{SD} bins, which have the same size in $\log(r_d)$. In each bin, a single value or dry radius is randomly selected and assigned to a single SD. Multiplicity of the SD is readily calculated from the initial aerosol size spectrum. Next, wet radius is initialized to be in equilibrium with the initial relative humidity. If the initial relative humidity is higher than 0.95, wet radii are initialized as if it was equal to 0.95. This procedure is performed for each spatial cell. This initialization algorithm gives a good representation of the initial size spectrum even for small values of N_{SD}.

Advection of SDs is modeled with a predictor-corrector algorithm described in Grabowski et al. (2018a). Simpler, first-order algorithms for advection were found to cause inhomogeneous spatial distributions of SDs, with less SDs in regions with high vorticity.

3.3 Order of operations

The sequence of operations done in a single time step is presented on a Unified Modeling Language (UML) sequence diagram in fig. 1. The diagram is a convenient way of showing how coupling between the Eulerian dynamics and the Lagrangian microphysics is done. The diagram also shows operations that are done simultaneously on CPUs and GPUs. Please note how the liquid water mixing ratio q_l is treated. In principle, liquid water is resolved by the SDM and could be diagnosed from the super-droplet size spectrum each time it is needed in the RHS. This would however require additional synchronization between CPUs and GPUs. To avoid this computational performance problem, we introduce an auxiliary Eulerian field for q_l. Its value is diagnosed from SDs after condensation and its advection is done using the first-order accurate upwind scheme.

3.4 Spatial discretization

All of the model dependent variables are co-located. Their positions form the nodes of the primary grid. However, the libmpdata++ advection algorithms are formulated using a dual, staggered Arakawa-C grid (Arakawa and Lamb, 1977). The cell centers of the dual grid are the nodes of the primary mesh. Schematic of a 2D computational domain with the Arakawa-C grid is shown in fig. 2. Throughout this paper, by "grid cells", "Eulerian cells" or simply "cells", we refer to the cells of the dual

Geosci. Model Dev. Discuss., https://doi.org/10.5194/gmd-2018-281
Manuscript under review for journal Geosci. Model Dev.
Discussion started: 4 February 2019

Geoscientific Model Development Discussions

grid. To form the Arakawa-C arrangement, components of the vector $\boldsymbol{u}$ are linearly interpolated to the edges of the dual grid (see Jaruga et al. (2015) for details). Super-droplets are restricted to the physical space, which is the shaded region in fig. 2. Coupling of the Eulerian variables with SDs is done using the dual grid. All SDs that are located in the same cell of the dual grid are subjected to the same conditions, which are equal to the values of scalars residing at the center of the cell. Similarly, condensation of a given SD affects scalars in the center of the dual grid cell, in which this SD is located. To calculate the velocity of air that advects a given SD, velocities, which reside at edges of the dual grid, are interpolated to the position of the SD. The interpolation is done linearly, separately in each dimension, as advocated by Grabowski et al. (2018a). Spatial discretization is also necessary in the algorithm for modeling collision-coalescence (cf. section 2.2). We use the dual grid cells also as coalescence cells, with the exception of the cells at domain edges. There, only the physical (shaded) part of dual grid cells is used as coalescence cells.

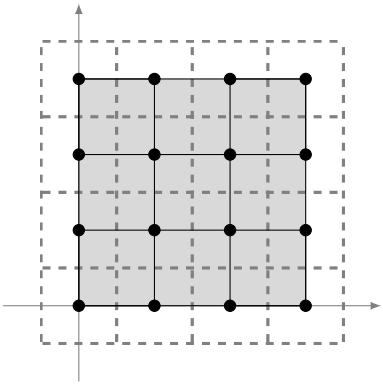

Figure 2. Schematic of a 2D computational domain. Bullets mark the data points for the dependent variable ψ in eq. (13), solid lines depict edges of primary grid and dashed lines mark edges of dual grid. Reproduced from Jaruga et al. (2015).

4 Comparison with other models - marine stratocumulus

UWLCM is validated by running simulations of a marine stratocumulus using a setup based on observations made during the second Dynamics and Chemistry of Marine Stratocumulus (DYCOMS-II) field study (Stevens et al., 2003). The setup, described in detail in Ackerman et al. (2009), is an idealization of conditions observed during the research flight 2 (RF02) of this campaign. Both heavily drizzling open cells and lightly drizzling closed cells were sampled by RF02. The initial thermodynamic conditions are an average from both types of cells and the microphysical conditions are an average over heavily drizzling cells only. Comparison of simulation results from 11 different LES models is presented in Ackerman et al. (2009). There is a large variability in the amount of drizzle in different models. It illustrates how difficult it is for LES models to reproduce drizzle formation. One of the reasons why we chose to test UWLCM using this setup is to test how well the Lagrangian microphysics performs in modeling drizzle. The models that took part in the intercomparison use either bin microphysics (one model with single-moment bin and one model with double-moment bin) or bulk microphysics (2 models with single-moment

Geosci. Model Dev. Discuss., https://doi.org/10.5194/gmd-2018-281
Manuscript under review for journal Geosci. Model Dev.
Discussion started: 4 February 2019

bulk and 7 models with double-moment bulk). Another difference between UWLCM and models discussed in Ackerman et al. (2009) is that the models from the intercomparison use explicit sub-grid scale (SGS) models, while UWLCM uses the implicit LES (iLES) approach (Grinstein et al., 2007). In the implicit LES approach, it is assumed that the numerical diffusion of the advection scheme is enough to reproduce diffusion due to the SGS mixing. The MPDATA algorithm is argued to be well-suited for iLES simulations (Margolin and Rider, 2002; Margolin et al., 2006). It is important to note that there is no subgrid-scale mixing of liquid water in UWLCM, because the liquid water is represented by Lagrangian particles.

4.1 Simulation setup

The simulation setup follows Ackerman et al. (2009). The domain size is 6.4km x 6.4km x 1.5km with a regular grid of cells of 50m x 50m x 5m size. Rigid and periodic boundary conditions are used at the vertical and horizontal edges of the domain, respectively. Simulations are run with two values of the time step length, $\Delta t = 1\text{s}$ and $\Delta t = 0.1\text{s}$. In simulations with $\Delta t = 1\text{s}$, 10 sub-steps for condensation are done per single time step. The simulations are run for 6 hours. The initial profiles of q_v and θ give high values of supersaturation in the layer, in which a cloud was observed. However, the simulation is initialized without any cloud water, because it is not known analytically what should be the initial wet radius distribution. First part of the simulation, called the *spinup* period, is dedicated to obtaining a stationary distribution of wet radii. During the spinup, the collision-coalescence process is turned off and the supersaturation in the condensational growth equation is limited to 1%. Please note that in (Ackerman et al., 2009) this supersaturation limit is applied only to the activation and not to the condensational growth. This approach can not be used in UWLCM, because in UWLCM activation is not modeled as a separate process. The spinup period is 1 hour long, which was found to be enough to reach a stationary concentration of cloud droplets, which should be a good proxy for having a stationary spectrum of the wet radius. Aerosol is assumed to consist of ammonium sulfate with the initial size distribution as defined in Appendix A of Ackerman et al. (2009). Following Petters and Kreidenweis (2007), the hygroscopicity parameter for ammonium sulfate is $\kappa = 0.61$. Surface fluxes are exponentially distributed in each column with a 25 m e-folding height. Collision efficiencies are taken from Hall (1980) for large droplets and from Davis (1972) for small droplets. Coalescence efficiency is set to 1. The terminal velocity is calculated using the formula from Khvorostyanov and Curry (2002). libmpdata++ allows the user to choose from a number of MPDATA options. In the presented simulations, we use the "infinite-gauge" option *iga* for handling variable-signed fields and the non-oscillatory option *fct*.

4.2 Two-dimensional simulations

The 2D simulations are used to investigate differences between the *per-cell* and *per-particle* substepping algorithms (see Sec. B), and to test sensitivity of results to the number of SDs. Simulations are done for $N_{\text{SD}} = 40$ (which is the number of SDs per cell also used in 3D simulations) and for $N_{\text{SD}} = 1000$. Results are compared with 3D simulations from the Ackerman et al. (2009) in order to assert if 2D simulations, which are computationally cheap, give reasonable representation of some of the features of 3D simulations. In 2D, we observed significant variability in results of simulation runs done for the same values of N_{SD}, Δt and using the same substepping algorithm. The variability comes from two sources. One is that the initial

Geosci. Model Dev. Discuss., https://doi.org/10.5194/gmd-2018-281
Manuscript under review for journal Geosci. Model Dev.
Discussion started: 4 February 2019

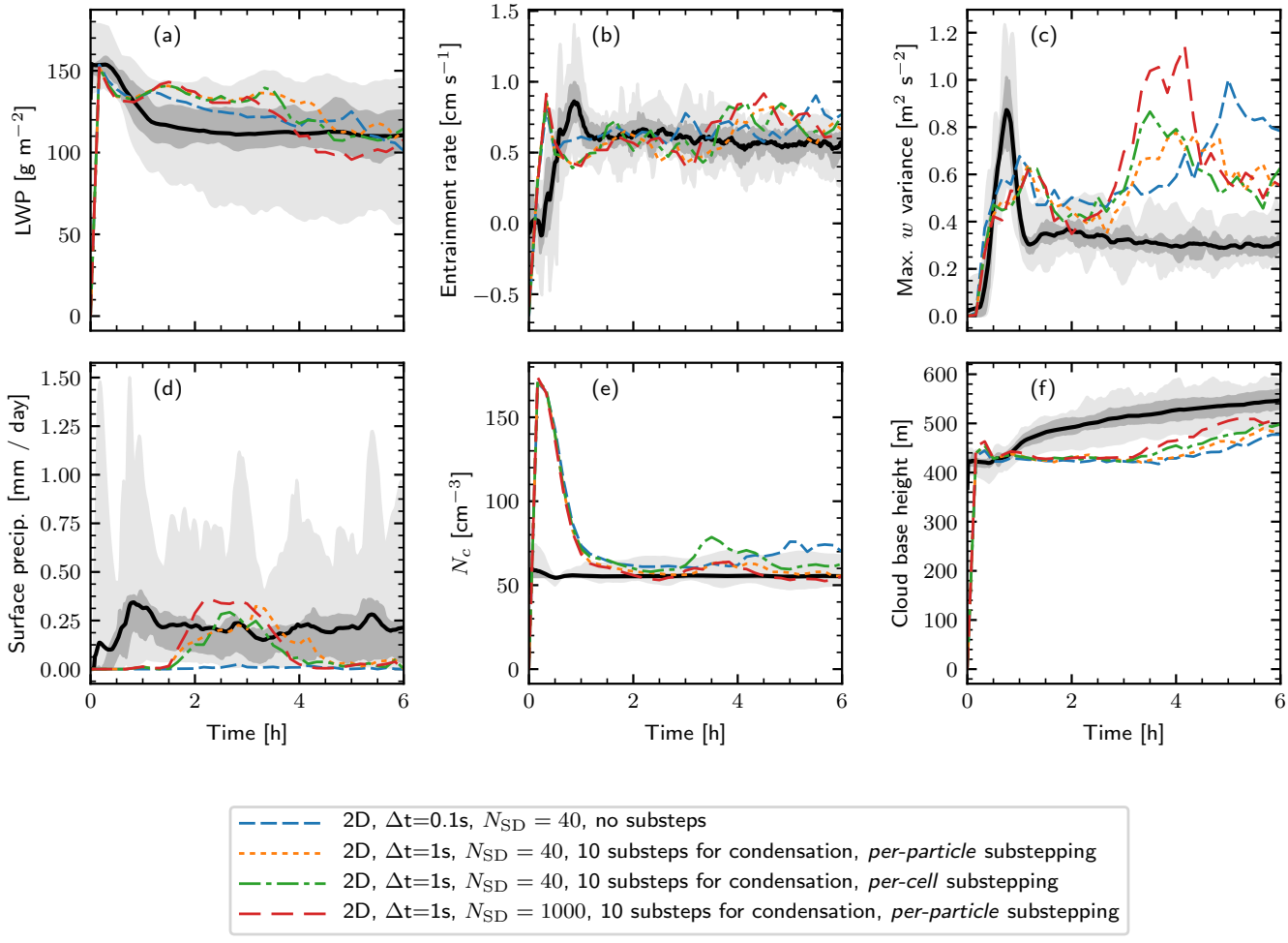

Figure 3. 2D UWLCM results. Time series of a domain averaged liquid water path, entrainment rate, maximum of vertical velocity variance, surface precipitation, concentration of cloud droplets in cloudy cells and cloud base height. UWLCM simulations were done for different values of time step length, number and type of sub-steps, and initial number of SDs per cell. Each colored line represents an average from 10 UWLCM simulations of a given type. Results of 3D simulations from an ensemble of 11 models are shown for reference (Ackerman et al., 2009). Mean, middle two quartiles, and range of that reference ensemble are plotted with the black solid line, the dark shaded region and the light shaded region, respectively.

thermodynamic conditions include a small random perturbation. The other is that initialization of SD radii and collision-coalescence of SDs are modeled with Monte Carlo algorithms. To compensate for this inherent variability, all shown UWLCM results of 2D simulations are averages from ensembles of 10 simulations.

Time series of selected domain-averaged variables are shown in fig. 3. The 3D simulations from Ackerman et al. (2009) are referred to as reference simulations. The amount of liquid water does not depend on Δt nor on N_{SD}. It slowly decreases with

Geosci. Model Dev. Discuss., https://doi.org/10.5194/gmd-2018-281
Manuscript under review for journal Geosci. Model Dev.
Discussion started: 4 February 2019

time, but is within the range of results of the reference simulations. The entrainment rate, which is calculated as the rate of increase of the inversion height, also agrees with the reference simulations, except for differences during the spinup period. However, there is a noticeable increase in the entrainment rate during the 3h - 5h period of the simulations with $\Delta t = 1$s. This increase coincides with a more pronounced increase in the maximum of variance of vertical velocity, which up to this point is in agreement with the reference simulations. This in turn is preceded by a period of increased surface precipitation from 2h to 4h of the simulation. That would suggest that the increase in the maximum of variance of w is caused by rain evaporation. This hypothesis is backed by the fact that simulations with most rain (for $N_{\mathrm{SD}} = 1000$) have the highest maximum of variance of w. However, for $\Delta t = 0.1$s, a sudden increase in the maximum of variance of w is also seen, albeit at a later period starting at 5 h, but is not preceded by an increase in the surface precipitation. It is probable that for $\Delta t = 0.1$s rain evaporation also drives the increase of VAR(w), but all rain drops evaporate before reaching the ground. Outside of the periods of increased precipitation that were discussed above, there is almost no surface precipitation in UWLCM simulations. There is a large spread in the amount of surface precipitation in the reference simulations, with some models producing as little rain as the 2D UWLCM. The need for the spinup period for microphysics is best seen on the N_c time series. Initially, due to the large initial supersaturation, cloud droplets form on all aerosol particles. Afterwards, N_c quickly decreases and after 1h arrives at the value of ca. 60 cm^{-3}. Then, the number of cloud droplets remains constant, aside of the periods with increased variance of w, when the activation rate increases. Concentration of cloud droplets after the spinup is in agreement with the reference simulations. It is worth to note that eight of the reference models do not predict the value of cloud droplet concentration, but use a fixed value $N_c = 55$ cm^{-3}. The cloud base height in 2D simulations remains constant until the third hour of simulation. Then it starts to increase and catches up with the reference simulations.

Vertical profiles from the 2D simulations are shown in fig. 4. Vertical distributions of liquid water, total water and liquid-water potential temperature do not depend on the time step length nor on the number of SDs, and are in agreement with reference simulations. Precipitation flux for $\Delta t = 1$s is similar to the smallest values of the reference results and is slightly higher for $N_{\mathrm{SD}} = 1000$ than for $N_{\mathrm{SD}} = 40$. A similar observation was made in Dziekan and Pawlowska (2017), where the mean autoconversion time was found to increase with decreasing N_{SD}. The most striking differences between the 2D UWLCM and 3D reference simulations are seen on the profiles of moments of the vertical velocity distribution. This is associated with the decreased dimensionality of our simulations. Interestingly, profiles of VAR(w) and of the third moment of w are in better agreement with observations (see fig. 3 in Ackerman et al. (2009)) in the 2D UWLCM than in the 3D reference simulations. It is worth to note that the profile of VAR(w) is not constant during the 2h - 6h period over which results in fig. 4 are averaged. Instead, it goes through significant changes with the maximum of VAR(w) varying between 0.4 $\mathrm{m}^2\mathrm{s}^{-2}$ and 1.2 $\mathrm{m}^2\mathrm{s}^{-2}$ (see fig. 3).

Differences between the *per-particle* and *per-cell* sub-stepping algorithms are visible on the profiles of N_c. Firstly, fewer cloud droplets are produced in the *per-particle* than in the *per-cell* case. Secondly, N_c within the cloud layer decreases with height in the *per-particle* case, but increases with height in the *per-cell* case. In simulations without sub-stepping and with $\Delta t = 0.1$s, a decrease in N_c with height is seen, which is in agreement with the *per-particle* sub-stepping. However,the *per-cell* sub-

Geosci. Model Dev. Discuss., https://doi.org/10.5194/gmd-2018-281
Manuscript under review for journal Geosci. Model Dev.
Discussion started: 4 February 2019

Geoscientific Model Development Discussions
Open Access
EGU

stepping gives values of N_c closer to the value obtained for $\Delta t = 0.1$s, but we consider it a coincidence, since supersaturation is higher in the $\Delta t = 0.1$s simulations.

Judging from results of 2D simulations, the *per-particle* substepping is necessary to properly represent condensational growth of SDs. Regarding the number of SDs, 2D simulations showed that using relatively few SDs ($N_{\mathrm{SD}} = 40$) does not affect the results, aside from a small decrease in the amount of precipitation.

4.3 Three-dimensional simulations

The 3D simulations were done for $N_{\mathrm{SD}} = 40$ and for two values of time step length, $\Delta t = 0.1$s without substepping and $\Delta t = 1$s with 10 substeps using the *per-particle* algorithm. Contrary to the 2D simulations, 3D simulations show very little variability between realizations thanks to a larger simulation domain. Therefore averaging over an ensemble of simulations, which was necessary in the 2D case, is not needed here and results shown come from a single simulation run. Time series of the results are shown in fig. 5. It is seen that the time step length has greater impact on 3D simulations than on 2D simulations. Nevertheless, results for both values of Δt are within the range of the reference simulations, with the exception of surface precipitation. Liquid-water path slowly decreases with time and is ca. 30% higher for $\Delta t = 1$s than for $\Delta t = 0.1$s. The entrainment rate is close to the highest values of the reference results, with slightly higher values for $\Delta t = 0.1$s than for $\Delta t = 1$s, which may be the cause why LWP is smaller in the former case. The maximum of VAR(w) is the same for both runs and is in very good agreement with the mean from the reference simulations. Like in 2D simulations, there is very little surface precipitation in the 3D runs. Concentration of cloud drops after the spinup period is in agreement with the reference simulations, although simulations with $\Delta t = 0.1$s give a little higher values of N_c than simulations with $\Delta t = 1$s. Contrary to the 2D results, cloud base height is in agreement with the reference simulations.

Profiles obtained from 3D simulations are presented in fig. 6. Regardless of the time step length, liquid-water potential temperature, total water mixing ratio and liquid-water mixing ratio are in agreement with reference simulations. Cloud fraction, which is the fraction of cells with $N_c > 20\ \mathrm{cm}^{-3}$, is slightly lower than in reference simulations, especially for $\Delta t = 0.1$s. Judging from the profile of N_c, average value of N_c in UWLCM is slightly higher than in the reference simulations. Therefore spatial variability in N_c has to be higher in UWLCM than in the reference models. The reason for this may be twofold. Firstly, there is no numerical diffusion of N_c in UWLCM, thanks to the use of Lagrangian microphysics. Secondly, the SDM used in UWLCM produces too high spatial variability, because it represents liquid water using a relatively small number of computational droplets. The precipitation flux is lower than in reference simulations. Variance of w does not depend on Δt and is in agreement with the reference simulations. The absolute value of the third moment of w is close to zero, in contrast to the reference results. The difference is potentially caused by the iLES approach used in UWLCM. Arguably, the third moment of w within cloud layer is in better agreement with observations than the reference simulations (observational results are plotted in Ackerman et al. (2009)). In the sub-cloud layer the contrary is true: the reference simulations are in better agreement with observations. The supersaturation profile for $\Delta t = 1$s is in agreement with reference results. For $\Delta t = 0.1$s supersaturation is a little lower than for $\Delta t = 1$s, which is the opposite of what was observed in 2D simulations. The concentration of cloud droplets is slightly higher than the mean of the reference results. As in the 2D case, N_c is a little higher for the shorter time step.

Geosci. Model Dev. Discuss., https://doi.org/10.5194/gmd-2018-281
Manuscript under review for journal Geosci. Model Dev.
Discussion started: 4 February 2019

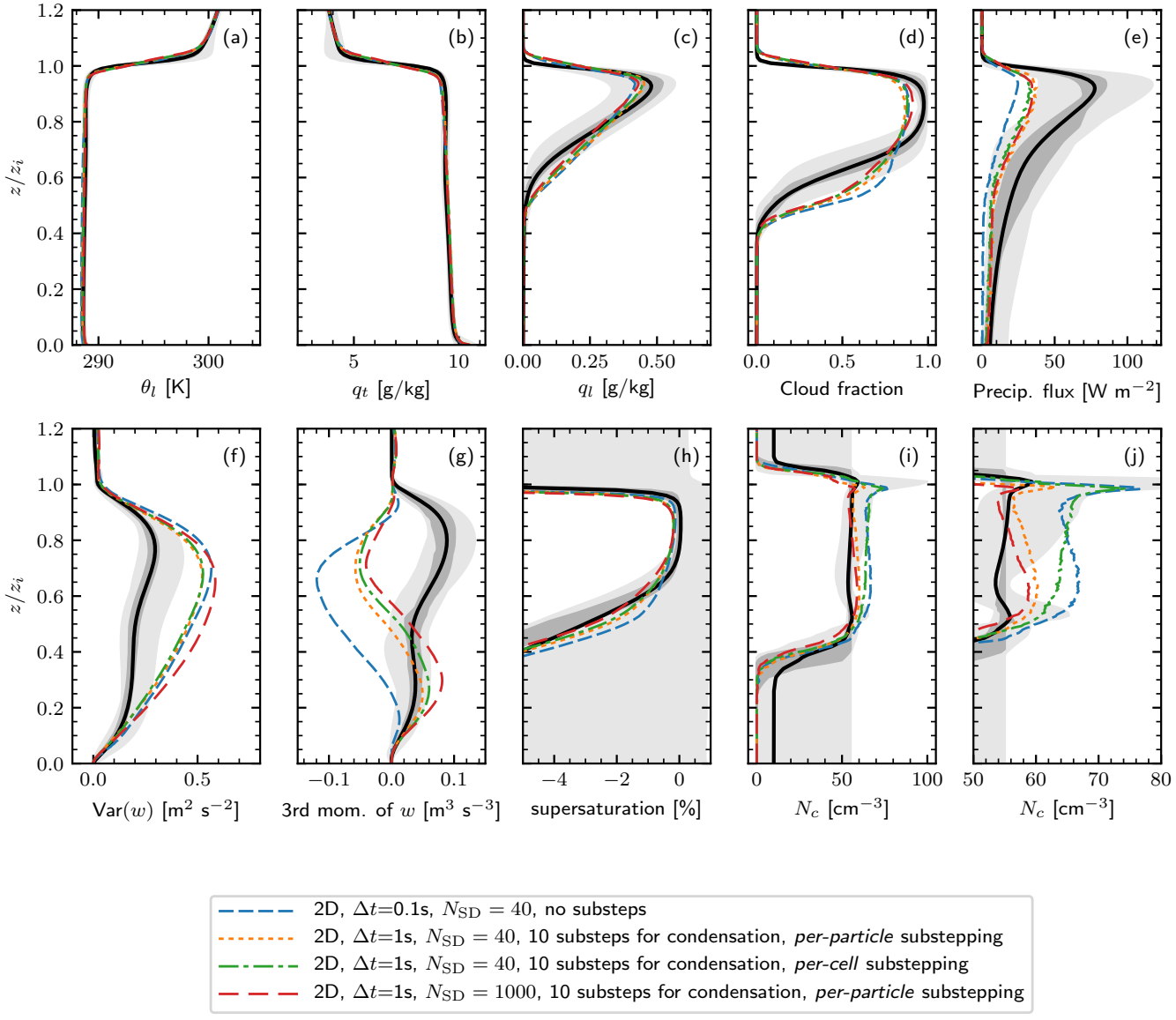

Figure 4. 2D UWLCM results. As in fig. 3, but showing horizontally-averaged profiles of liquid water potential temperature (defined in Ackerman et al. (2009)), total water mixing ratio, liquid water mixing ratio, cloud fraction (defined in appendix A), precipitation flux (defined in appendix A), variance of vertical velocity, third moment of vertical velocity, supersaturation and concentration of droplets in cloudy cells, which is shown on the two panels with different scales of the horizontal axis. On the vertical axis is height normalized by the inversion height. The profiles are averaged over the 2h to 6h period.

Geosci. Model Dev. Discuss., https://doi.org/10.5194/gmd-2018-281
Manuscript under review for journal Geosci. Model Dev.
Discussion started: 4 February 2019

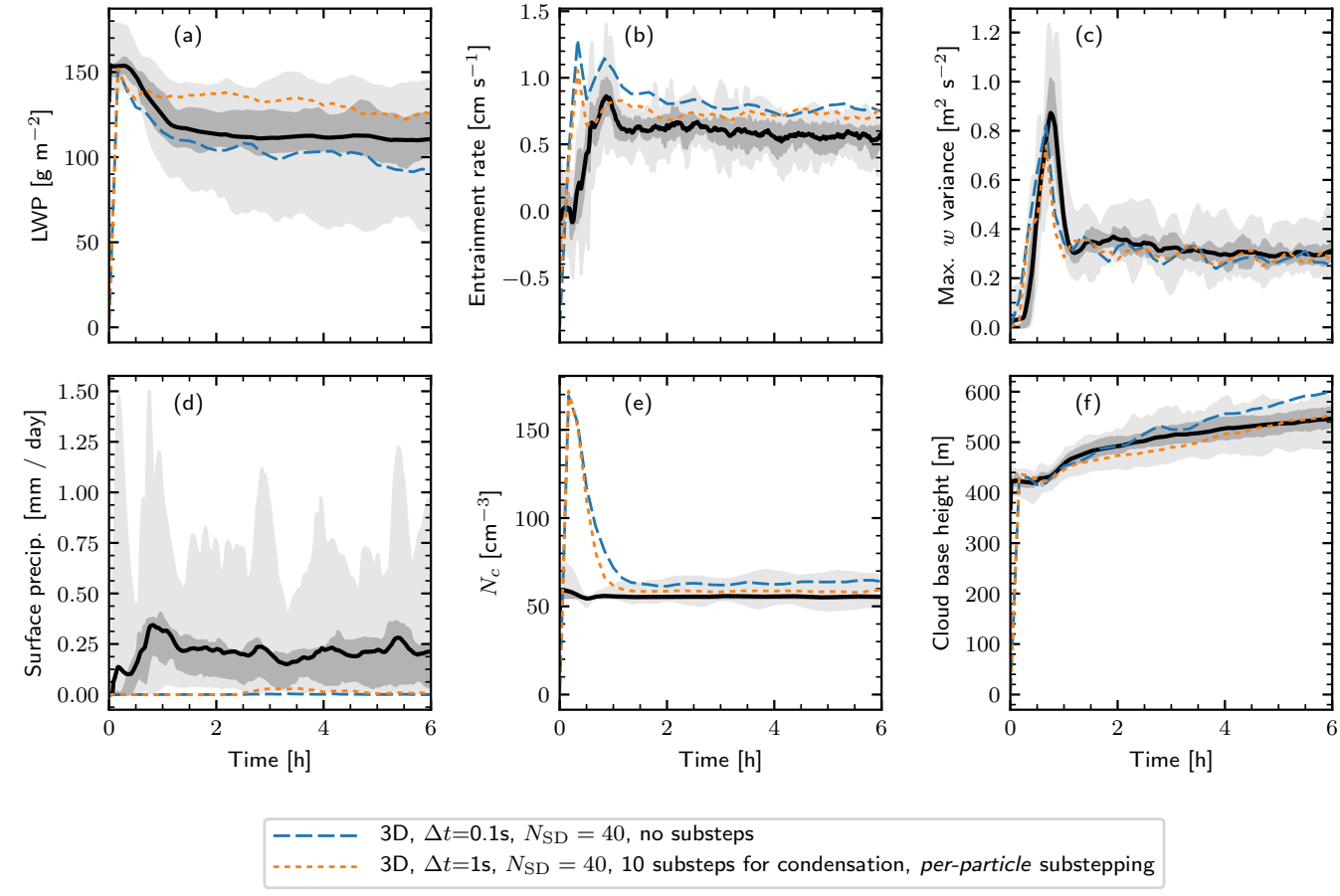

Figure 5. As in fig. 3, but for 3D UWLCM simulations. No averaging over ensembles is done, i.e. each line comes from a single UWLCM run.

Droplet activation rate near the cloud top is higher for $\Delta t = 0.1$s than for $\Delta t = 1s$, possibly due to a better resolved maxima of supersaturation at the cloud top or a better resolved time of residence of aerosols near the cloud top. Finally, it is seen that droplet activation near the cloud base happens at higher altitudes than in most of the reference simulations.

4.4 Precipitation results

The purpose of this section is to study the discrepancy between the amount of surface precipitation observed during the DYCOMS-II campaign (from ca. 0.25 mm/day to ca. 0.45 mm/day, Ackerman et al. (2009)) and modeled by UWLCM (almost none). The precipitation flux in UWLCM is ca. two times lower than the average of reference simulations (cf. fig. 6). We suspect that the reason is that the number of cloud droplets is a little higher in UWLCM. To check if this is the case, a simulation with a decreased concentration of aerosols is presented. We also make a comparison with the only models with

Geosci. Model Dev. Discuss., https://doi.org/10.5194/gmd-2018-281
Manuscript under review for journal Geosci. Model Dev.
Discussion started: 4 February 2019

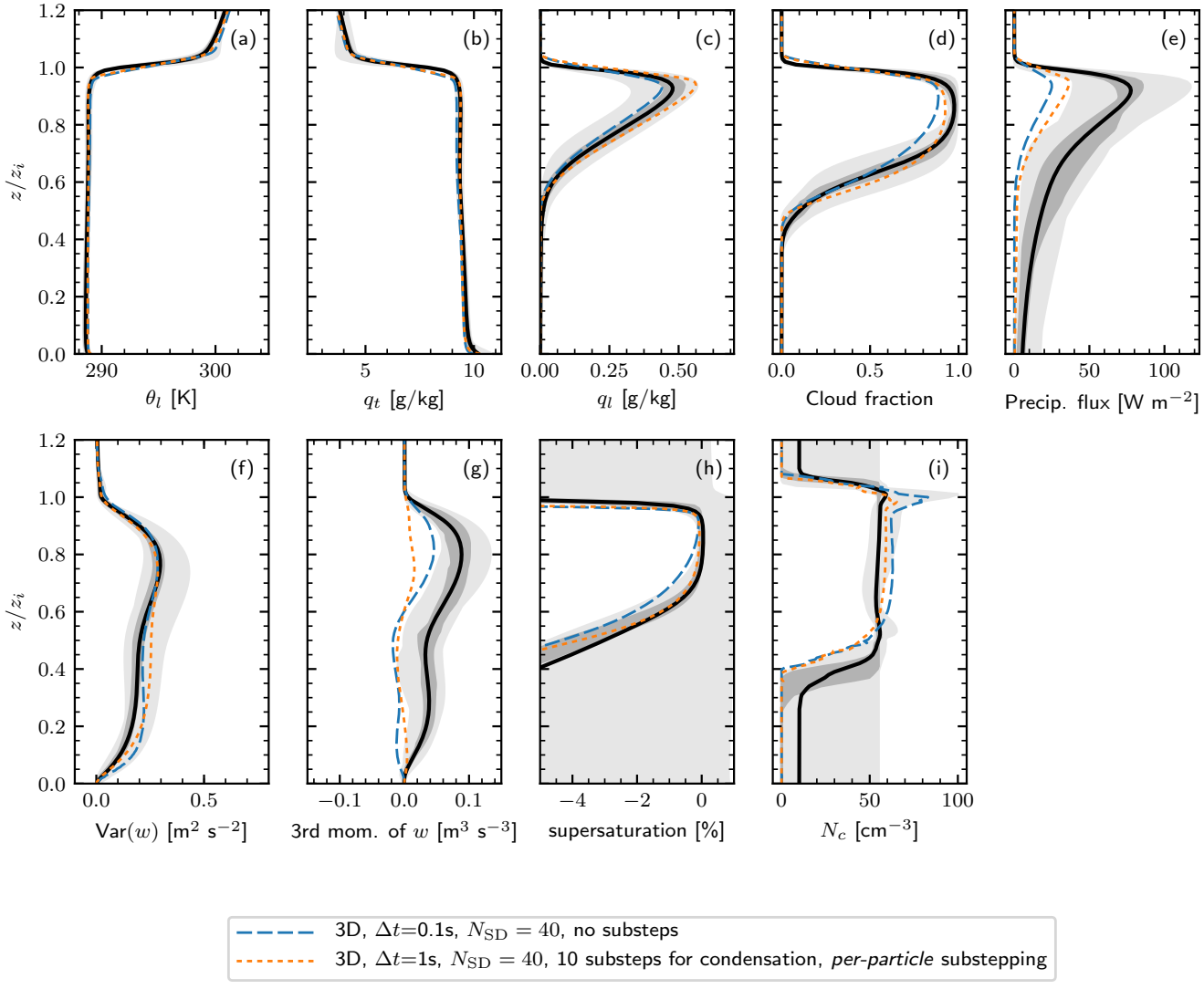

Figure 6. As in fig. 4, but for 3D UWLCM simulations. No averaging over ensembles is done, i.e. each line comes from a single UWLCM run.

Geosci. Model Dev. Discuss., https://doi.org/10.5194/gmd-2018-281
Manuscript under review for journal Geosci. Model Dev.
Discussion started: 4 February 2019

bin microphysics that took part in the reference intercomparison: Distributed Hydrodynamic Aerosol and Radiative Modeling Application (DHARMA) and Regional Atmospheric Modeling System (RAMS). DHARMA uses single-moment bin microphysics, while RAMS uses double-moment bin microphysics. We compare only with these two models, because, contrary to the bulk schemes, bin schemes explicitly resolve the size spectrum and do not rely on parametrisations of the collision-coalescence process, i.e. they are at a similar level of precision as the SDM. Bin microphysics are troubled by artificial broadening of the size spectrum of droplets due to numerical diffusion associated with advection in the physical space (Morrison et al., 2018). Such artificial broadening increases the rate of collision-coalescence, hence models with bin microphysics might produce too much drizzle. Lagrangian, particle-based schemes have no numerical diffusion in the size spectrum.

Time series and profiles showing the amount of liquid water, surface precipitation and concentration of cloud droplets from UWLCM, DHARMA and RAMS are plotted in fig. 7. In addition to the UWLCM run already shown in figs. 5 and 6, which we will refer to as the default UWLCM, we present a UWLCM simulation in which the initial concentration of aerosols in the larger mode is $45\ \mathrm{cm}^{-3}$ (default value is $65\ \mathrm{cm}^{-3}$). Surface precipitation in the RAMS model is close to zero, aside from a short period at the start of the simulation, when the simulation has not yet reached a stationary state. This result is in agreement with the default UWLCM simulation. The DHARMA model stands out in that the amount of surface precipitation it produces is higher, in agreement with observations. It might seem that the reason why it produces more precipitation is that the concentration of cloud droplets is lower than in the default UWLCM or RAMS. However, the UWLCM simulation with lower aerosol concentration produces even lower concetration of cloud droplets than DHARMA, but does not give as much surface precipitation. The total amount of liquid water is in good agreement between DHARMA and UWLCM. Together, this suggests that the large amount of surface precipitation in DHARMA may be caused by the artificial broadening of spectra caused by numerical diffusion.

4.5 Explicit modeling of activation

In UWLCM, droplet activation is modeled explicitly, in contrast to the models with bin microphysics, which parametrise this process. Difference between these two approaches is apparent in the profile of N_c in fig. 7. DHARMA and RAMS models predict local maxima of N_c near the cloud base, where supersaturation is the heighest. This is because parametrisations of activation assume that it is an instantaneous process, therefore even a short-lived maximum of supersaturation results in activation of new droplets. In UWLCM, thanks to the explicit treatment of activation, time scale of activation is resolved and the local maximum of supersaturation near cloud base does not cause activation of new droplets. Therefore N_c in UWLCM monotonously increases near the cloud base. The activation height is in good agreement between UWLCM and RAMS. In DHARMA activation takes place at a much lower altitude.

4.6 Aerosol processing

The SDM models spectrum not only of the wet radius, but also of the dry radius. This makes it ideal for studying processing of aerosols in clouds. One example is an effect observed in the time series of N_c in fig. 7. The UWLCM simulation with decreased initial aerosol concentration predicts a slow decrease of N_c with time. We interpret it as a manifestation of depletion of large

Geosci. Model Dev. Discuss., https://doi.org/10.5194/gmd-2018-281
Manuscript under review for journal Geosci. Model Dev.
Discussion started: 4 February 2019

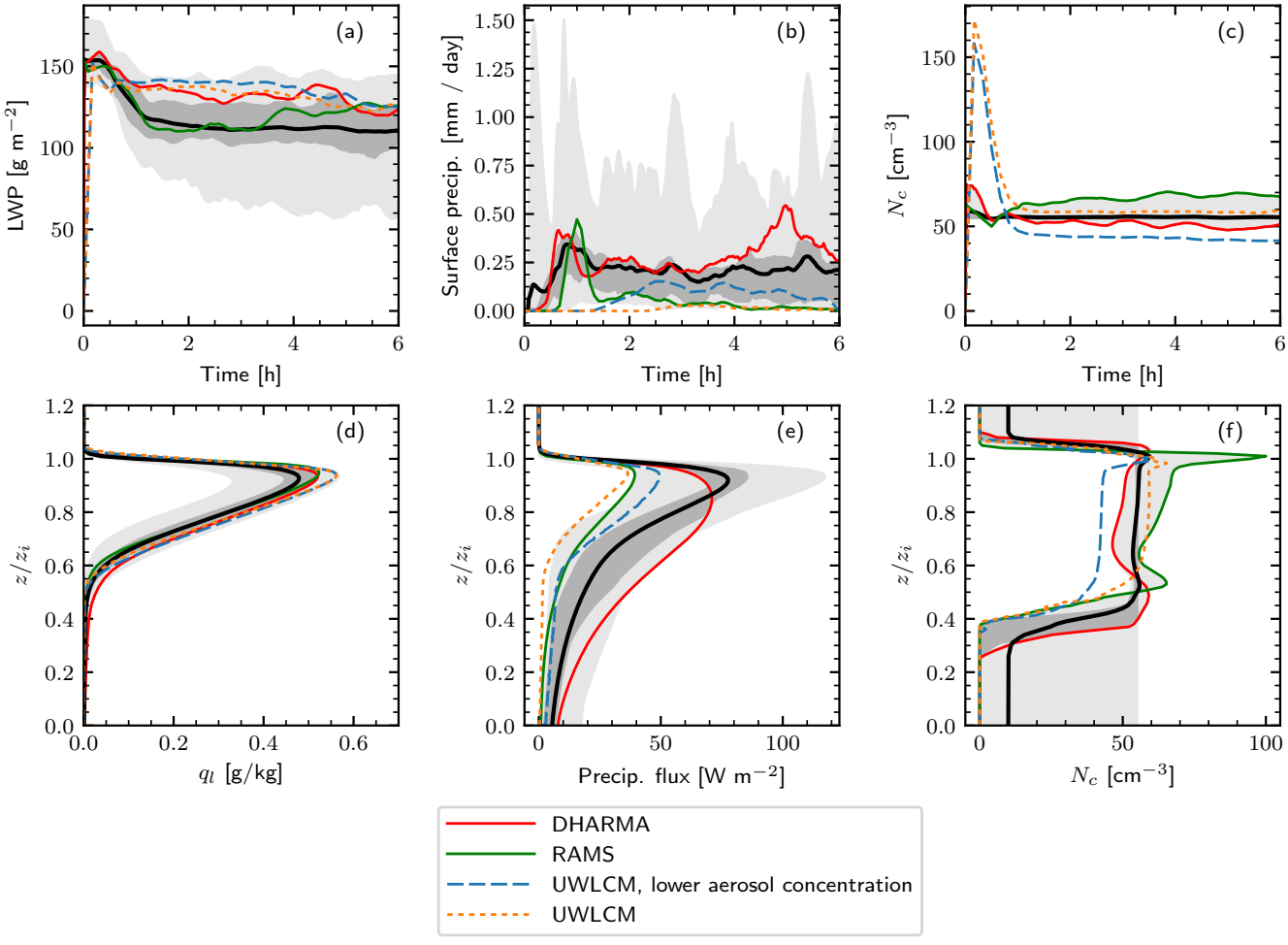

Figure 7. Selected time series of domain averages (upper row) and vertical profiles (lower row) from the 3D UWLCM and the two models with bin microphysics that took part in the Ackerman et al. (2009) intercomparison: DHARMA and RAMS. UWLCM results come from a 3D simulations with $\Delta t = 1$s and 10 *per-particle* sub-steps. The "lower concentration" run of UWLCM uses a decreased concentration of aerosols in the larger mode, 45 cm^{-3} (default value is 65 cm^{-3}). Out of the two DHARMA runs done for the intercomparison, the DHARMA_BO run is shown, because it uses coalescence efficiency closer to unity, which is the value used in UWLCM and RAMS. Profiles are averaged and scaled as in fig. 4. Reference results from all models discussed in Ackerman et al. (2009) are depicted as in fig. 4.

aerosols, which are washed out with surface precipitation. Then, less large aerosols are present, hence less cloud droplets are formed. In the default UWLCM simulation, in which there is no surface precipitation, N_c remains constant in time.

Geosci. Model Dev. Discuss., https://doi.org/10.5194/gmd-2018-281
Manuscript under review for journal Geosci. Model Dev.
Discussion started: 4 February 2019

5 Summary

We have presented a new large-eddy simulations model with a Lagrangian particle-based cloud microphysics. The model was build by combining two open-source libraries, one for handling the Eulerian dynamics and the other implementing the Lagrangian microphysics scheme. Methods for coupling the Lagrangian microphysics with the Eulerian dynamics were presented, including spatial discretizations, a sub-stepping algorithm and an algorithm for simultaneous computations of the Eulerian and Lagrangian components. Simulations of a marine stratocumulus have shown that the model gives results in agreement with reference results from 11 other LES models. The model was found to work well with a 1s time step. Two-dimensional and three-dimensional simulations of the stratocumulus setup were performed. The two-dimensional simulations with UWLCM were shown to give reasonable results regarding microphysical phenomena at a fraction of the computational cost of the three-dimensional simulations. Number of computational particles used in the Lagrangian microphysics was not found to have impact on domain averages, apart from a small increase in the amount of surface precipitation. Surface precipitation modeled by UWLCM is lower than in most models with bulk microphysics. Compared to models with bin microphysics, surface precipitation in UWLCM is in agreement with the RAMS model, but smaller than in the DHARMA model. In UWLCM, all particles, including humidified aerosols, evolve according to the same set of equations. Therefore it is not necessary to include droplet activation as an additional process. Advantages of such approach are most apparent near the cloud base, where bin schemes discussed produce local maxima of cloud droplet concentration, while in UWLCM cloud droplet concentration increases monotonously. A discrepancy in the third moment of the vertical velocity was found between UWLCM and the reference models. Probably, this discrepancy is due to the implicit LES approach used in UWLCM, while all the reference models use explicit SGS schemes. This hypothesis will be tested once explicit SGS schemes are added to UWLCM. Implementation of the Smagorinsky scheme is currently under development. Other extensions of UWLCM that we are working on include a distributed-memory implementation, addition of a single-moment and double-moment microphysics schemes and addition of a SGS scheme for condensation (Grabowski and Abade, 2017).

6 Code availability

UWLCM, libmpdata++ and libcloudph++ codes are available at https://github.com/igfuw.

7 Data availability

For simulation results, please contact P. Dziekan.

Appendix A: List of symbols

Geosci. Model Dev. Discuss., https://doi.org/10.5194/gmd-2018-281
Manuscript under review for journal Geosci. Model Dev.
Discussion started: 4 February 2019

Geoscientific Model Development Discussions
Open Access
EGU

Table A1. List of symbols. As in Ackerman et al. (2009), cloudy cells are those with concentration of cloud droplets greater than 20 cm^{-3}. Cloud droplets are liquid particles with radius in the range $0.5\ \mu\mathrm{m} < r < 25\ \mu\mathrm{m}$. Cloud fraction is the ratio of cloudy cells to the total number of cells. Precipitation flux in a cell is calculated as $\left(\sum \xi \frac{4}{3}\pi r^3 w_t\right) \rho_w l_v / V$, where V is volume of the grid cell and the sum is done over all SDs in the cell.

Symbol	SI unit	Description
$\theta = T(p_{1000}/p)^{\frac{R_d}{c_{pd}}}$	[K]	potential temperature
$p_{1000} = 10^5$	[Pa]	reference pressure
θ_v	[K]	virtual potential temperature
$\theta_l = (p_{1000}/p)^{\frac{R_d}{c_{pd}}}(T - l_{v0}\frac{q_l}{c_{pd}})$	[K]	liquid-water potential temperature
R_d, R_v	[J K^{-1} kg^{-1}]	gas constants for dry air/water vapor
$c_\mathrm{pd} = 1005$	[J K^{-1} kg^{-1}]	specific heat at const. pressure for dry air
$l_{v0} = 2.5 \times 10^6$	[J kg^{-1}]	latent heat of evaporation at the triple point
$q_v = m_v/m_d$, q_{vs}	[kg kg^{-1}]	water vapor mixing ratio/saturation vapor mixing ratio
q_l, $q_t = q_v + q_l$	[kg kg^{-1}]	liquid-water/total water mixing ratio
m_v, m_d	[kg]	mass of water vapor / dry air
$\boldsymbol{u} = (u, v, w)$	[m s^{-1}]	velocity field in Cartesian coordinates
$\pi = (p - p^e)/\rho_d^r$	[m^{2}s^{-2}]	normalized pressure perturbation
$\boldsymbol{k}$	[1]	vertical unit vector
B	[m s^{-2}]	buoyancy
F_X	[(unit of X) s^{-1}]	forcing of X (surface fluxes, radiation, absorbers, subsidence, ...)
X^e, X^r	[(unit of X)]	environmental/reference profile of X
$l_v(T)$	[J kg^{-1}]	latent heat of evaporation (cf. Arabas et al. (2015))
E_c, E_e, $C = E_c - E_e$	[s^{-1}]	condensation/evaporation rate and their balance
g	[m s^{-2}]	magnitude of Earth's gravitational acceleration
$\epsilon = R_v/R_d - 1$	[1]	
ρ, ρ_d	[kg m^{-3}]	density of air/dry air
$S = \mathrm{d}_z\theta_v/\theta_v$	[m^{-1}]	non-dimensional stability of the atmosphere
$\boldsymbol{x} = (x, y, z)$	[m]	Cartesian coordinates
r, r_d	[m]	wet/dry radius of a SD
κ	[1]	hygroscopicity parameter of a SD
ξ	[1]	multiplicity of a SD
e_s	[Pa]	saturation partial pressure of vapor
N_c	[m^{-3}]	concentration of cloud droplets in cloudy grid cells
N_SD	[1]	initial number of SDs per grid cell
Δt	[s]	time step length of the dynamical core
z_i	[m]	mean height of the $q_t = 8$ g kg^{-1} isosurface
w_t	[m s^{-1}]	terminal velocity of a SD
w_LS	[m s^{-1}]	large-scale subsidence velocity
ρ_w	[kg m^{-3}]	density of water

Geosci. Model Dev. Discuss., https://doi.org/10.5194/gmd-2018-281
Manuscript under review for journal Geosci. Model Dev.
Discussion started: 4 February 2019

Geoscientific Model Development Discussions

Appendix B: Condensation sub-stepping algorithm

Consider condensation of SDs within cell i at time step n. Vector of thermodynamic conditions in that cell at the moment right before condensation is calculated is denoted by $\boldsymbol{\psi}_i^{[n]} = \left(\theta^{[n]}, q_v^{[n]}\right)_i$. Number of time steps is denoted by S_c and sub-steps are indexed by ν, starting at $\nu = 1$. Super-droplets within cell i are numbered by μ. Vector of thermodynamic conditions that a given SD experiences at sub-step ν is denoted by $\breve{\boldsymbol{\psi}}_\mu^{[\nu]}$. Using this notation, the sub-stepping algorithm is

$$\breve{\boldsymbol{\psi}}_\mu^{[\nu+1/2]} = \breve{\boldsymbol{\psi}}_\mu^{[\nu]} + \frac{\boldsymbol{\psi}_i^{[n]} - \breve{\boldsymbol{\psi}}_\mu^{[\nu=1]}}{S_c}, \tag{B1}$$

$$r_\mu^{2[\nu+1]} = r_\mu^{2[\nu]} + \frac{\Delta t}{S_c} \left.\frac{dr^2}{dt}\right|_{r_\mu^{2[\nu+1]}, \breve{\boldsymbol{\psi}}_\mu^{[\nu+1/2]}}, \tag{B2}$$

$$\breve{\boldsymbol{\psi}}_\mu^{[\nu+1]} = \breve{\boldsymbol{\psi}}_\mu^{[\nu+1/2]} + \boldsymbol{A} \frac{4}{3} \frac{\pi \rho_w V}{\rho_d^r} \sum_{\mu=1}^{\mu=N_i^{[n]}} \xi_\mu \left[\left(r_\mu^{2[\nu+1]}\right)^{3/2} - \left(r_\mu^{2[\nu]}\right)^{3/2} \right], \tag{B3}$$

where r_μ^2 is the square of the wet radius of the μ-th SD, $N_i^{[n]}$ is the number of SDs in cell i at time step n and $\boldsymbol{A} = \left(\theta^e l_v / \left(c_{pd} T^e\right), -1\right)$. Sum in eq. (B3) is done over all SDs in cell i at time step n. For details of the predictor-corrector algorithm for calculation of the change of radius in eq. (B2), see Eqs. (17)-(19) in Arabas et al. (2015). After the last sub-step, the value of $\breve{\boldsymbol{\psi}}_\mu^{[\nu=S_c]}$ is the same for all SDs in the cell and the condensational RHS returned from the condensation algorithm is

$$R_c^{[n]} = \frac{\breve{\boldsymbol{\psi}}_{\mu=1}^{[\nu=S_c]} - \boldsymbol{\psi}_i^{[n]}}{\Delta t}. \tag{B4}$$

The initial value $\breve{\boldsymbol{\psi}}_\mu^{[\nu=1]}$ is equal to the thermodynamic conditions after condensation finished in the previous time step. Two ways of defining $\breve{\boldsymbol{\psi}}_\mu^{[\nu=1]}$ are considered, which differ in the spatial cell from which this initial condition is diagnosed:

$$\breve{\boldsymbol{\psi}}_\mu^{[\nu=1]} = \left(\boldsymbol{\psi}^{[n-1]} + R_c{}^{[n-1]}\right)_{i(n-1)}, \tag{B5}$$

referred to as *per-particle* sub-stepping, and

$$\breve{\boldsymbol{\psi}}_\mu^{[\nu=1]} = \left(\boldsymbol{\psi}^{[n-1]} + R_c{}^{[n-1]}\right)_{i(n)}, \tag{B6}$$

what we call *per-cell* sub-stepping. The notation $i(n)$ stands for the index of the cell in which the μ-th SD was at time step n. The *per-cell* sub-stepping is less accurate, but requires less computational time and uses less memory. The reason is that in the *per-cell* method, all SDs in a given cell have the same values of $\breve{\boldsymbol{\psi}}_\mu^{[\nu]}$. Moreover, values of pressure and density do not need to be sub-stepped in the *per-cell* method, since they are constant in time in each cell.

Appendix C: Software implementation

UWLCM is written in the C++ language. It relies heavily on two C++ libraries developed by the cloud modeling group at the University of Warsaw: libmpdata++ (Jaruga et al., 2015) for the Eulerian component and libcloudph++ (Arabas et al., 2015)

Geosci. Model Dev. Discuss., https://doi.org/10.5194/gmd-2018-281
Manuscript under review for journal Geosci. Model Dev.
Discussion started: 4 February 2019

for the Lagrangian component of the model. Structure of the libmpdata++ and libcloudph++ codes and how they are used in UWLCM is schematically depicted in Fig. C1.

libmpdata++ is a set of solvers for the generalized transport equations that use the MPDATA advection scheme. The solvers are organized in a hierarchy, ordered from solvers for simple flows to solvers for more complex flows. Each more complex solver inherits from the simpler solver in the hierarchy. Such design simplifies code development, maintenance and reusability. Apart from the hierarchy of solvers, libmpdata++ contains three other independent modules: boundary conditions, concurrency handlers and output handlers, all of which are used in UWLCM.

libcloudph++ is an implementation of three microphysical models: SDM, a single-moment bulk model and a double-moment bulk model. The SDM is implemented using the Thrust library and the CUDA programming language. Thanks to that, the SDM can be run on multi-threaded CPUs as well as on multiple GPUs.

UWLCM code is built on top of the libmpdata++ solvers. Separate parts of the UWLCM code handle different types of simulations. The ”piggybacking” code makes it possible to run kinematic simulations, i.e. simulations with a prescribed velocity field. The ”2D/3D” part of the code handles the dimensionality of the problem. The ”forcings” code specifies external forcings, so it is the part of the code that depends on simulation setup. The ”microphysics” module is responsible for handling the choice of microphysics (only Lagrangian microphysics is available in the current UWLCM release). Thanks to such code structure, different types of simulations, e.g. 2D and 3D simulations, different simulation setups or kinematic simulations, are using mostly the same source code. The highest performance is achieved when UWLCM is run on a system with GPUs. In that case, the Eulerian component is calculated on CPUs and the Lagrangian component on GPUs. Large part of these computations is done simultaneously (cf. fig. 1). The UWLCM code is open-source, under a version-control system and available from a git repository. Model output is done in the HDF5 format, ready for plotting in *Paraview*. UWLCM also includes simple software for plotting time series and vertical profiles. A number of test programs was developed for UWLCM, libcloudph++ and libmpdata++. UWLCM currently can run in parallel only on shared-memory systems. An implementation for distributed-memory systems is currently under development. UWLCM code is inspired by the *icicle* kinematic model developed by S. Arabas and A. Jaruga (https://github.com/igfuw/libcloudphxx/models/kinematic_2D).

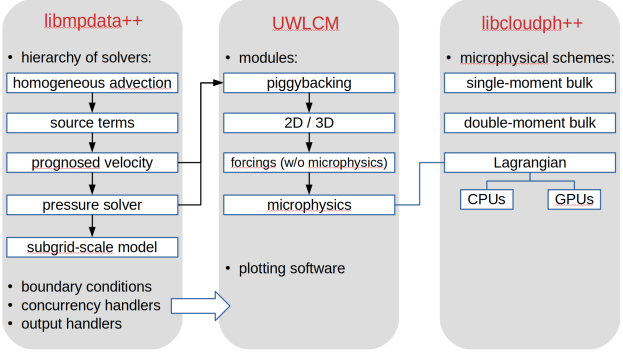

Figure C1. Schematic depiction of the structure of the code of UWLCM, libmpdata++ and libcloudph++. Black arrows denote inheritance between classes.

Geosci. Model Dev. Discuss., https://doi.org/10.5194/gmd-2018-281
Manuscript under review for journal Geosci. Model Dev.
Discussion started: 4 February 2019

Geoscientific Model Development Discussions
Open Access
EGU

Author contributions. PD developed the model code with contributions from MW. PD performed the simulations. PD and HP prepared the manuscript with contributions from MW.

Acknowledgements. We thank Wojciech Grabowski for discussions about the model formulation and about the manuscript. We are grateful to the AGH Cyfronet computation center for providing computing power. This research was supported by the Polish National Science Center grant 2016/23/B/ST10/00690.

References

Ackerman, A. S., vanZanten, M. C., Stevens, B., Savic-Jovcic, V., Bretherton, C. S., Chlond, A., Golaz, J.-C., Jiang, H., Khairoutdinov, M., Krueger, S. K., Lewellen, D. C., Lock, A., Moeng, C.-H., Nakamura, K., Petters, M. D., Snider, J. R., Weinbrecht, S., and Zulauf, M.: Large-Eddy Simulations of a Drizzling, Stratocumulus-Topped Marine Boundary Layer, Monthly Weather Review, 137, 1083–1110, https://doi.org/10.1175/2008MWR2582.1, https://doi.org/10.1175/2008MWR2582.1, 2009.

Andrejczuk, M., Reisner, J., Henson, B., Dubey, M., and Jeffery, C.: The potential impacts of pollution on a nondrizzling stratus deck: Does aerosol number matter more than type?, Journal of Geophysical Research: Atmospheres, 113, 2008.

Andrejczuk, M., Grabowski, W., Reisner, J., and Gadian, A.: Cloud-aerosol interactions for boundary layer stratocumulus in the Lagrangian Cloud Model, Journal of Geophysical Research: Atmospheres, 115, 2010.

Arabas, S. and Pawlowska, H.: Adaptive method of lines for multi-component aerosol condensational growth and CCN activation, Geoscientific Model Development, 4, 15–31, https://doi.org/10.5194/gmd-4-15-2011, https://www.geosci-model-dev.net/4/15/2011/, 2011.

Arabas, S. and Shima, S.-i.: Large-eddy simulations of trade wind cumuli using particle-based microphysics with Monte Carlo coalescence, Journal of the Atmospheric Sciences, 70, 2768–2777, 2013.

Arabas, S., Jaruga, A., Pawlowska, H., and Grabowski, W.: libcloudph++ 1.0: a single-moment bulk, double-moment bulk, and particle-based warm-rain microphysics library in C++, Geoscientific Model Development, 8, 1677–1707, 2015.

Arakawa, A. and Lamb, V. R.: Computational design of the basic dynamical processes of the UCLA general circulation model, General circulation models of the atmosphere, 17, 173–265, 1977.

Clark, T. L. and Farley, R. D.: Severe Downslope Windstorm Calculations in Two and Three Spatial Dimensions Using Anelastic Interactive Grid Nesting: A Possible Mechanism for Gustiness, Journal of the Atmospheric Sciences, 41, 329–350, https://doi.org/10.1175/1520-0469(1984)041<0329:SDWCIT>2.0.CO;2, https://doi.org/10.1175/1520-0469(1984)041<0329:SDWCIT>2.0.CO;2, 1984.

Davis, M. H.: Collisions of small cloud droplets: Gas kinetic effects, Journal of the Atmospheric Sciences, 29, 911–915, 1972.

Dziekan, P. and Pawlowska, H.: Stochastic coalescence in Lagrangian cloud microphysics, Atmospheric Chemistry and Physics, 17, 13 509–13 520, https://doi.org/10.5194/acp-17-13509-2017, https://www.atmos-chem-phys.net/17/13509/2017/, 2017.

Gillespie, D. T.: The stochastic coalescence model for cloud droplet growth, Journal of the Atmospheric Sciences, 29, 1496–1510, 1972.

Grabowski, W. W. and Abade, G. C.: Broadening of Cloud Droplet Spectra through Eddy Hopping: Turbulent Adiabatic Parcel Simulations, Journal of the Atmospheric Sciences, 74, 1485–1493, https://doi.org/10.1175/JAS-D-17-0043.1, 2017.

Grabowski, W. W. and Smolarkiewicz, P. K.: Two-Time-Level Semi-Lagrangian Modeling of Precipitating Clouds, Monthly Weather Review, 124, 487–497, https://doi.org/10.1175/1520-0493(1996)124<0487:TTLSLM>2.0.CO;2, https://doi.org/10.1175/1520-0493(1996)124<0487:TTLSLM>2.0.CO;2, 1996.

Grabowski, W. W., Dziekan, P., and Pawlowska, H.: Lagrangian condensation microphysics with Twomey CCN activation, Geoscientific Model Development, 11, 103–120, https://doi.org/10.5194/gmd-11-103-2018, https://www.geosci-model-dev.net/11/103/2018/, 2018a.

Grabowski, W. W., Morrison, H., Shima, S.-i., Abade, G., Pawlowska, H., and Dziekan, P.: Modeling of cloud microphysics: Can we do better?, Bulletin of the American Meteorological Society, https://doi.org/https://doi.org/10.1175/BAMS-D-18-0005.1, 2018b.

Grinstein, F. F., Margolin, L. G., and Rider, W. J.: Implicit large eddy simulation: computing turbulent fluid dynamics, Cambridge university press, 2007.

Hall, W. D.: A detailed microphysical model within a two-dimensional dynamic framework: Model description and preliminary results, Journal of the Atmospheric Sciences, 37, 2486–2507, 1980.

Hoffmann, F., Raasch, S., and Noh, Y.: Entrainment of aerosols and their activation in a shallow cumulus cloud studied with a coupled LCM–LES approach, Atmospheric Research, 156, 43 – 57, https://doi.org/https://doi.org/10.1016/j.atmosres.2014.12.008, http://www.sciencedirect.com/science/article/pii/S016980951400444X, 2015.

Hoffmann, F., Noh, Y., and Raasch, S.: The route to raindrop formation in a shallow cumulus cloud simulated by a Lagrangian cloud model, Journal of the Atmospheric Sciences, 74, 2125–2142, 2017.

Jaruga, A., Arabas, S., Jarecka, D., Pawlowska, H., Smolarkiewicz, P. K., and Waruszewski, M.: libmpdata++ 1.0: a library of parallel MPDATA solvers for systems of generalised transport equations, Geoscientific Model Development, 8, 1005–1032, https://doi.org/10.5194/gmd-8-1005-2015, https://www.geosci-model-dev.net/8/1005/2015/, 2015.

Khvorostyanov, V. I. and Curry, J. A.: Terminal Velocities of Droplets and Crystals: Power Laws with Continuous Parameters over the Size Spectrum, Journal of the Atmospheric Sciences, 59, 1872–1884, https://doi.org/10.1175/1520-0469(2002)059<1872:TVODAC>2.0.CO;2, https://doi.org/10.1175/1520-0469(2002)059<1872:TVODAC>2.0.CO;2, 2002.

Klein, R., Achatz, U., Bresch, D., Knio, O. M., and Smolarkiewicz, P. K.: Regime of validity of soundproof atmospheric flow models, Journal of the Atmospheric Sciences, 67, 3226–3237, 2010.

Lipps, F. B. and Hemler, R. S.: A Scale Analysis of Deep Moist Convection and Some Related Numerical Calculations, Journal of the Atmospheric Sciences, 39, 2192–2210, https://doi.org/10.1175/1520-0469(1982)039<2192:ASAODM>2.0.CO;2, https://doi.org/10.1175/1520-0469(1982)039<2192:ASAODM>2.0.CO;2, 1982.

Margolin, L., Smolarkiewicz, P., and Wyszogradzki, A.: Dissipation in implicit turbulence models: A computational study, Journal of applied mechanics, 73, 469–473, 2006.

Margolin, L. G. and Rider, W. J.: A rationale for implicit turbulence modelling, International Journal for Numerical Methods in Fluids, 39, 821–841, 2002.

Morrison, H., Witte, M., Bryan, G. H., Harrington, J. Y., and Lebo, Z. J.: Broadening of modeled cloud droplet spectra using bin microphysics in an Eulerian spatial domain, Journal of the Atmospheric Sciences, https://doi.org/10.1175/JAS-D-18-0055.1, https://doi.org/10.1175/JAS-D-18-0055.1, 2018.

Naumann, A. K. and Seifert, A.: A Lagrangian drop model to study warm rain microphysical processes in shallow cumulus, Journal of Advances in Modeling Earth Systems, 7, 1136–1154, 2015.

Petters, M. D. and Kreidenweis, S. M.: A single parameter representation of hygroscopic growth and cloud condensation nucleus activity, Atmospheric Chemistry and Physics, 7, 1961–1971, https://doi.org/10.5194/acp-7-1961-2007, https://www.atmos-chem-phys.net/7/1961/2007/, 2007.

Riechelmann, T., Noh, Y., and Raasch, S.: A new method for large-eddy simulations of clouds with Lagrangian droplets including the effects of turbulent collision, New Journal of Physics, 14, 065 008, 2012.

Shima, S.-i., Kusano, K., Kawano, A., Sugiyama, T., and Kawahara, S.: The super-droplet method for the numerical simulation of clouds and precipitation: A particle-based and probabilistic microphysics model coupled with a non-hydrostatic model, Quarterly Journal of the Royal Meteorological Society, 135, 1307–1320, 2009.

Smolarkiewicz, P. and Margolin, L.: Variational methods for elliptic problems in fluid models, in: Proc. ECMWF Workshop on Developments in numerical methods for very high resolution global models, pp. 137–159, 2000.

Smolarkiewicz, P. K.: Multidimensional positive definite advection transport algorithm: an overview, International Journal for Numerical Methods in Fluids, 50, 1123–1144, https://doi.org/10.1002/fld.1071, https://onlinelibrary.wiley.com/doi/abs/10.1002/fld.1071, 2006.

Smolarkiewicz, P. K.: Modeling atmospheric circulations with soundproof equations, in: Proc. of the ECMWF Workshop on Nonhydrostatic Modelling, 8-10 November, 2010, Reading, UK, pp. 1–15, 2011.

Smolarkiewicz, P. K. and Szmelter, J.: A nonhydrostatic unstructured-mesh soundproof model for simulation of internal gravity waves, Acta Geophysica, 59, 1109, 2011.

Smolarkiewicz, P. K., Kühnlein, C., and Wedi, N. P.: A consistent framework for discrete integrations of soundproof and compressible PDEs of atmospheric dynamics, Journal of Computational Physics, 263, 185 – 205, https://doi.org/https://doi.org/10.1016/j.jcp.2014.01.031, http://www.sciencedirect.com/science/article/pii/S0021999114000588, 2014.

Stevens, B., Lenschow, D. H., Vali, G., Gerber, H., Bandy, A., Blomquist, B., Brenguier, J. L., Bretherton, C. S., Burnet, F., Campos, T., Chai, S., Faloona, I., Friesen, D., Haimov, S., Laursen, K., Lilly, D. K., Loehrer, S. M., Malinowski, S. P., Morley, B., Petters, M. D., Rogers, D. C., Russell, L., Savic-Jovcic, V., Snider, J. R., Straub, D., Szumowski, M. J., Takagi, H., Thornton, D. C., Tschudi, M., Twohy, C., Wetzel, M., and van Zanten, M. C.: Dynamics and Chemistry of Marine Stratocumulus—DYCOMS-II, Bulletin of the American Meteorological Society, 84, 579–594, https://doi.org/10.1175/BAMS-84-5-579, https://doi.org/10.1175/BAMS-84-5-579, 2003.

Unterstrasser, S., Hoffmann, F., and Lerch, M.: Collection/aggregation algorithms in Lagrangian cloud microphysical models: rigorous evaluation in box model simulations, Geoscientific Model Development, 10, 1521, 2017.